Proportional-and-Hysteretic-Damping Control: a Human Inspired Method for Robot Impedance

Nicolas Brissonneau[1], Binghan He, Gray C. Thomas, Junhyeok Ahn and Luis Sentis

***Abstract*— Human muscles have a remarkable ability to maintain a constant damping ratio even as the inertia they carry changes. Inspired by this phenomenon, this study investigates its robotic reproduction via a nonlinear controller we call Proportional-and-Hysteretic-Damping or PHD control. While the effect is easier to explain in the frequency domain, we provide an implementable approximation in the time-domain. For comparison, we demonstrate superior robustness to inertia changes relative to the classic Proportional-Derivative or PD controllers. This comparison is performed on a simple physical testbed, and then scaled to a simulation of a line-foot bipedal robot. In both cases the new controller demonstrates the human-like robustness to inertia changes.**

I. Introduction

Hysteretic damping is an extensively studied phenomenon of dissipation of energy for which scientific interest has peaked in structural and civil engineering sciences. It is mostly studied in the frequency domain where its properties have been demonstrated and replicated in passive components and systems [1] [2]. While [3] has identified the hysteretic spring model in the human elbow joints, these results were recently strengthened by [4] as they allowed for better human-adapted controller design for exoskeletons. But it does not seem to be restrained to humans as [5] have shown that cockroaches' legs actually fit a hysteretic damping model over a wide range of frequencies too. One of the key features of a hysteretic damping model is its unique property of having a frequency independent damping ratio, which means that it improves a system's robustness against overshoot provoked by unknown inertia variations. On one hand, we are curious as to the benefits such model provides to the human body's dynamics and we aim at sharing its properties with robots by designing a new PHD control strategy. On another hand, questions arise regarding its implementation potential in robotics as its non-linear nature makes it non trivial to represent in the time-domain in the first place. Linear-hysteretic-damping models are studied like the Kelvin and Maxwell elements and Hilbert transformation in the time-domain[6] [7]. Since Hilbert transformation is non-causal, other approaches aimed to realize the hysteretic damping through a causal relaxation [8], an additional all-pass filter in the frequency domain [9], and a triangular approximation of the hysteresis loop [10]. Similar to the triangular hysteresis loop approximation, the problems addressed by this PHD implementation have been considered in the field of adaptive control which already investigates how to react to the very changes of the system we are trying to control [11] [12] [13]. But while adaptive control aims at identifying model uncertainties and compensating for untracked disturbances, a strength of a hysteretic damping-based controller lies in the absence of any identification requirements, the position and velocity configurations of the robot are sufficient knowledge for the controller.

In this paper we investigate how to transfer to robotics systems this feature identified in human joints dynamics. First, we provide a parameterized time-domain approximation of a complex stiffness, which is based on a nonlinear hysteresis effect. Then, we demonstrate the applicable concept of a damping invariant control law with the implementation of a PHD-based impedance controller on a 1-DoF system and show results in simulation and hardware. Finally, we address the scalability to multi-dof systems by maintaining the bipedal robot DRACO's standing balance.

II. Proportional-and-Hysteretic-Damping

For a linear second order oscillatory system like a Mass-Spring-Damper (MSD), a Laplace-transformed representation would be

$$\frac{\tau}{q} = \frac{1}{ms^2 + bs + k}, \tag{1}$$

where b the linear damping coefficient, k the stiffness, m the mass of the system, q the displacement and τ the external torque applied to the system. We have natural frequency and damping ratio expressed as $\omega_0 = \sqrt{k/m}$ and $\zeta = b/(2\sqrt{km})$.

The complex stiffness model [4] differs from the MSD model by introducing a frequency-dependent damping behavior $b = h/\omega$. By substituting $s = j\omega$, it is simplified to

$$\frac{\tau}{q} = \frac{1}{ms^2 + jh + k} \tag{2}$$

which results in a mass-invariant damping ratio $\zeta = h/2k$.

A. Mass Invariant Damping Ratio via Mass-Dependent Damping Matrix

We first consider modeling a system's interactions with its environment linearly and adjusting its damping matrix, B, to provide a constant damping ratio by taking advantage of our estimate of the contact constrained mass matrix Λ

This work was supported by the U.S. Government, NASA Space Technology Research Fellowship NNX15AQ33H, the Office of Naval Research, ONR Grant N000141512507 and the National Science Foundation, NSF Grant 1724360. We thank the members of the Human Centered Robotics Lab, University of Texas at Austin who provided insight and expertise that assisted the research. Authors are with The Departments of Mechanical Engineering (N.B., B.H., G.C.T., J.A.) and Aerospace Engineering (L.S.), University of Texas at Austin, Austin, TX. Send correspondence to [1] nicolasb@utexas.edu.

$$\Lambda^{-1} = M^{-1} - M^{-1}J_c^T(J_cM^{-1}J_c^T)^{-1}J_cM^{-1} \quad (3)$$

$$M_c = (J_e\Lambda^{-1}J_e^T)^{-1} = LL^T \quad (4)$$

$$W^2 = L^{-1}KL^{-T} \quad (5)$$

$$B = 2L\zeta WL^T \quad (6)$$

where Λ is the contact constrained mass matrix, M is the floating base mass matrix, J_c is the contact Jacobian, M_c is the contact constrained operational space mass matrix, J_e is the environment's contact Jacobian, L is the Cholesky decomposition of M_c, and W, ζ, K and B are the parameters under matrix form of a multi-dof mass-spring-damper system.

However, this model relies heavily on the knowledge of the environment and has thus weak guarantees of achieving the expected result outside of a simulation environment.

B. Mass Invariant Damping Ratio via Nonlinear Hysteretic Damping

If the controller does not know the inertia of the environment, the contact configuration, or the mass of the robot accurately, is it still possible to achieve a mass invariant damping ratio? We have then explored the perspective of designing a nonlinear controller which approximates the frequency domain behavior of a complex stiffness—what we call PHD control. To emulate a complex stiffness, the control needs to be dominated by spring-like behavior, but maintain a constant phase lag independent of frequency. This type of phase lag behavior can be achieved by hysteresis, but hysteresis as typically implemented is also a highly amplitude dependent behavior that adds less and less phase lag as the input gets larger. Our model essentially scales the amount of hysteresis as a function of the spring deflection in order to avoid having an amplitude-dependent behavior. A spring model with two switching stiffness is a good start as both behaviors are linear and therefore do not introduce an amplitude dependence by themselves.

First, we can model a hysteretic spring force by adding a hysteretic damping one shaped as a hyperbola to the force originating from the real stiffness

$$f_{Hyperbola} = kq + \text{sign}(\dot{q})\sqrt{\lambda + (\beta kq)^2}; \quad (7)$$

where λ changes the distance between the two focuses of the hyperbola. As λ increases, the two possible combined stiffness move away from the spring origin.

Secondly, the hysteretic spring component of (2) has actually been approximated in the time domain by Reid [10] with the non-causal model

$$f_{HS} = k\left(1 + \text{sign}(q\dot{q})\frac{\eta\pi}{2}\right)q \quad (8)$$

with η the frequency-independent loss factor. This approximation corresponding to $f_{Hyperbola}$ when $\lambda = 0$, we transformed (8) into the more adaptable form (9) in order to study a broad range of applications of this model for future implementations.

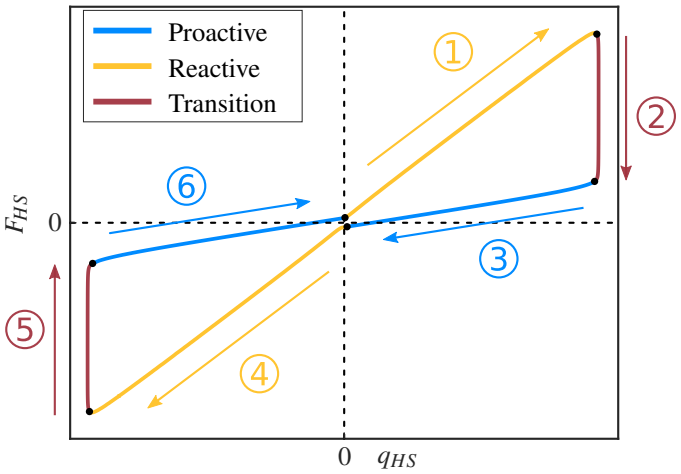

Fig. 1. Principle

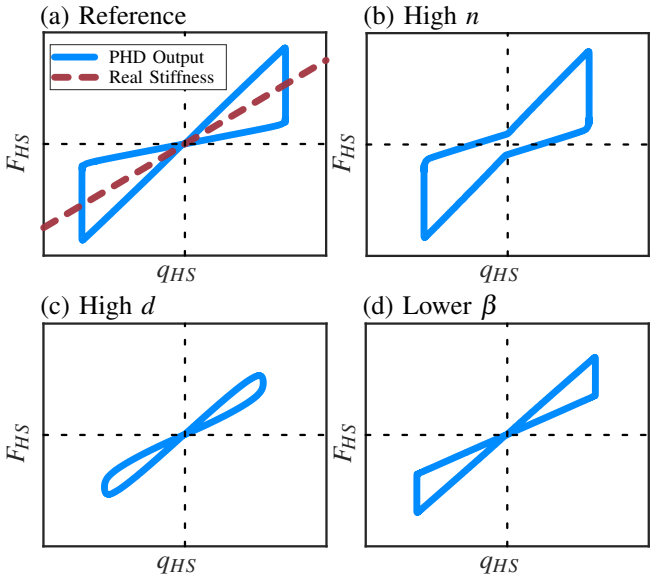

Fig. 2. Parameters Influence

$$f_{HS} = kq + \frac{(k\beta|q| + n)\dot{q}}{|\dot{q}| + d} \quad (9)$$

where $\beta = (1-\varepsilon)/(1+\varepsilon)$ for $\varepsilon \in (-1, 1]$. Based on the velocity sign we notice a switch between two effective stiffness, from an impedance controller perspective, this translates into a "*proactive*" and a "*reactive*" stiffness shown in Fig. 1. This design choice is meant to facilitate its integration as a controller of a realistic actuated system, it will prove to be particularly useful in our hardware implementation as it allows for a linear dynamic at low frequency while $|\dot{q}| < d$, avoids to cross a singular torque value with $n > 0$, β adjusts the deviation between the active and reactive stiffness, respectively $k(1-\beta)$ and $k(1+\beta)$, and together d and n allow for "smoothing" the two effective stiffness. One can have a better intuition of these parameters with Fig. 2.

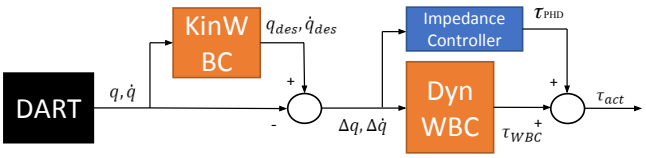

Fig. 3. Simulation structure

III. 1-DOF Simulation and Experiment

A. Simulation

To demonstrate that our time-domain approximation conserves the properties of a hysteretic spring, we simulate a 1-DoF actuated system which can be summarized as an immovable motor providing a perfect torque source τ in order to move a rod of known inertia J using an impedance controller. We define $\Delta q = q_{des} - q$, $\Delta \dot{q} = \dot{q}_{des} - \dot{q}$, our PHD controller's equation is

$$\tau_{PHD} = k\Delta q + \frac{(k\beta|\Delta q| + n)\Delta \dot{q}}{|\Delta \dot{q}| + d} \tag{10}$$

The simulation equations are shown below, with τ_g the torque applied by gravity, τ_{gcomp} the predicted gravity compensation torque representing the uncertainty on the system's mass:

$$\ddot{q} = \frac{1}{J}(\tau_g + \tau_{gcomp} + \tau_{PHD}) \tag{11}$$

To demonstrate our PHD controller's hysteretic damping robustness to inertia variations, we identify our system's frequency-domain model by adding an excitation exponential chirp τ_{chirp} covering the range of frequencies from 0.05 to 5 Hz while keeping $q_{des} = cst$. (8) becomes

$$\ddot{q} = \frac{1}{J}(\tau_g + \tau_{gcomp} + \tau_{PHD} + \tau_{chirp}). \tag{12}$$

We then tune a classic PD impedance controller to reach a similar gain magnitude plot as our PHD controller by sharing the same stiffness and by tuning the damping term accordingly, respectively b and β for PD and PHD. Now that our systems are "synced" in the frequency domain through their bode plots, we vary the inertia (and thus the natural frequency) by adding a mass to the rod and updating τ_{gcomp} accordingly. As shown in the figures below we use two masses $m1 = 0.66kg$ and $m2 = 4.56kg$ to compare each controller's sensitivity to changing their natural frequency.

The first set of takes out of Fig. 5 are visual. Even though the natural frequency changes, it is equivalent to translating the plot horizontally for our PHD controller's frequency-invariant damping. Also, the PD plots show that the rod's inertia increase in Fig. 5(a) naturally results in an increasingly damped behavior, and in Fig. 5(b) it results in an under-damped behavior prone to overshooting.

The second set of takes is the estimation of the damping ratio we are interested in. We have considered two approaches for quantifying the damping ratio, the first one is through fitting a MSD and the complex stiffness model in the frequency domain with the data gathered and compute:

$$\zeta = \zeta_{MSD} + \zeta_{MHD} = \frac{b}{2\sqrt{km}} + \frac{h}{2k} \tag{13}$$

The other approach consists in deriving the damping ratio from the energy dissipated over a loop, corresponding to the area close by the said loop in the torque to displacement graphs:

$$E_{dissipated} = \pi q_m^2 h$$
$$\zeta = \frac{h}{2k} \tag{14}$$

Even though the first approach seems more robust since it takes all frequencies into account, it is not always adequate to sweep over a wide range of frequencies. We verified our time-domain hysteretic damping performance in simulation and proceed to real hardware experimentation.

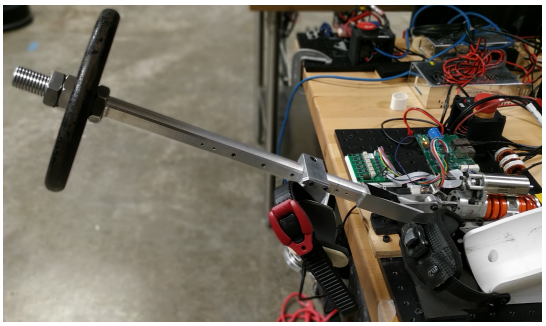

Fig. 4. P0 setup

B. Hardware

The following hardware experiments have been conducted on the Series-Elastic Actuator (SEA) P0 from Fig. 4, provided by the company Apptronik. While in the previous simulation we have assumed a perfect torque source and sensor data, using real hardware involves dealing with noise and inaccuracy in our models, the purpose of Fig. 6 is to introduce the reader to these constraints, it shows a set of data recorded during a chirp signal experiment described in III-A. Fig. 6(b) is a zoom-in on the red rectangle in Fig. 6(a), while Fig. 6(d),(e) and (f) show the torque readings in joint space corresponding to the 3 range of frequencies, highlighted in red in Fig. 6(c).

Fig. 6(b) justifies the choice of a high d term to relieve the system from its sensitivity to low frequency disturbances and the implementation of a second order low pass filter with $w_c = 120rad/s$ to avoid high frequency noise which would both lead to chattering. By giving a close look at the data in Fig. 6(d) we notice the proactive and reactive stiffness are very close, this is because we have linearized our model in low frequencies by increasing d. In Fig. 6(e), we have reached the system's nominal frequency and the torque's and displacement's amplitudes are at a maximum, the shape is non-mistakenly hysteretic so d is now too small to linearize the system's dynamics and this is crucial at this frequency as we want to avoid overshooting. Toward the high frequencies we notice the bias torque originating from the misestimation

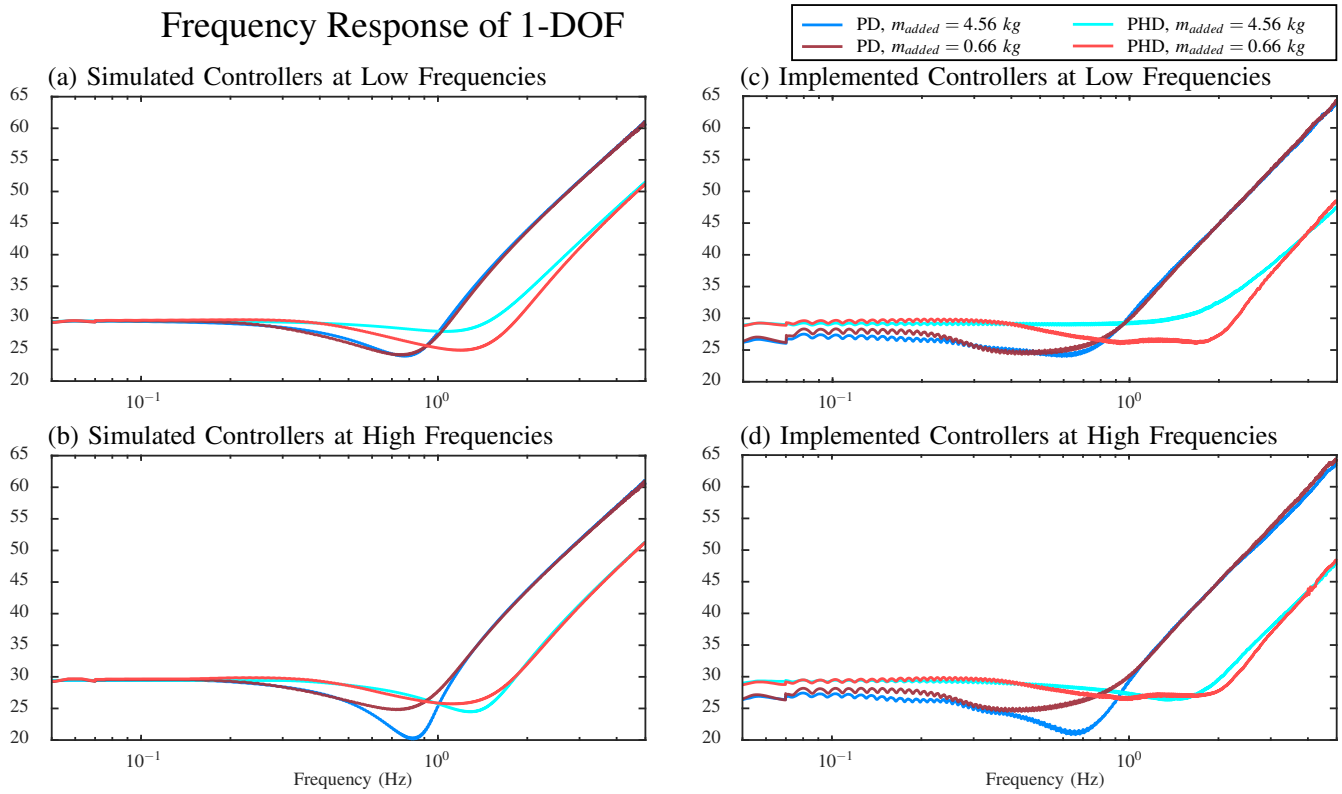

Fig. 5. Controllers sensitivity to inertia changes

of the gravity, as the damping is dependent of the equilibrium it becomes more pronounced and the inertia effects are now curving the profile of the plot.

IV. Multi-DOF Simulation

We are using DART simulation environment [14] and a humanoid robot as a testing application. DRACO is liquid-cooled viscoelastic biped and has ten actuated DOFs including three for the hip structure, one for the knee and one for the ankle [15].

The control structure we are using to demonstrate our controller's characteristics on the bipedal robot DRACO is a modified Whole-Body Locomotion Controller (WBLC) from [16] which is presented in Fig. 3. It consists of an inverted kinematics prediction (KinWBC) of the robot's desired configuration, based on a set of predefined tasks, which is put in series with an inverted dynamics model (DynWBC) predicting the torques required to drive the robot from its current configuration to the desired one while optimizing for 3 constraints: feet contact forces, feet acceleration and configuration relaxation.

WBLC is a Quadratic Programming (QP) which can be expressed as

$$\text{minimize} \quad F_r^T W_r F_r + \ddot{x}_c^T W_c \ddot{x}_c + \delta_{\ddot{q}}^T W_{\ddot{q}} \delta_{\ddot{q}} \tag{15}$$

$$\text{subject to} \quad UF_r \geq 0, \tag{16}$$

$$SF_r \leq F_{r,z-max}, \tag{17}$$

$$\ddot{x}_c = J_c^T \ddot{q} + \dot{J}_c \dot{q}, \tag{18}$$

$$A\ddot{q} + b + g = \begin{pmatrix} \mathbf{0}_{6\times 1} \\ \tau_{WBC} \end{pmatrix} + J_c^T F_r, \tag{19}$$

$$\ddot{q} = \ddot{q}_{WBC} + \delta_{\ddot{q}}, \tag{20}$$

$$\ddot{q}_{WBC} = \ddot{q}_{des} + k_d(\dot{q}_{des} - \dot{q}) + k_p(q_{des} - q), \tag{21}$$

$$\tau_{min} \leq \tau_{WBC} \leq \tau_{max}. \tag{22}$$

One can find a more detailed description of the controller in [16]. For the specific purpose of considering the scalability of our PHD controller to multi-DoF systems in simulation, we design a PHD alternative to both the PD low-level controller and the PD desired acceleration controller for the inverted dynamics computation. We share the equations for the desired joint acceleration PHD controller, the definition of τ_{WBC} and the actuator output τ_{act} which adds a vector of τ_{PHD} to τ_{WBC}

$$\ddot{q}_{des} = k\Delta q + \frac{(k\beta|\Delta q| + n)\Delta\dot{q}}{|\Delta\dot{q}| + d} \tag{23}$$

$$M\ddot{q}_{des} + b + g = \tau_{WBC} + J_c{}^t F_r \tag{24}$$

$$\tau_{act} = \tau_{WBC} + \tau_{PHD} \tag{25}$$

We set the following task: keeping the center of mass of the robot at a desired altitude between its two feet, and maintaining the initial hip orientation. DRACO's study case is very different from P0's in many ways, we are now balancing a floating base from a robot with contact constraints which do not guarantee anymore the forces transmission to the ground in case of jumping or slipping.

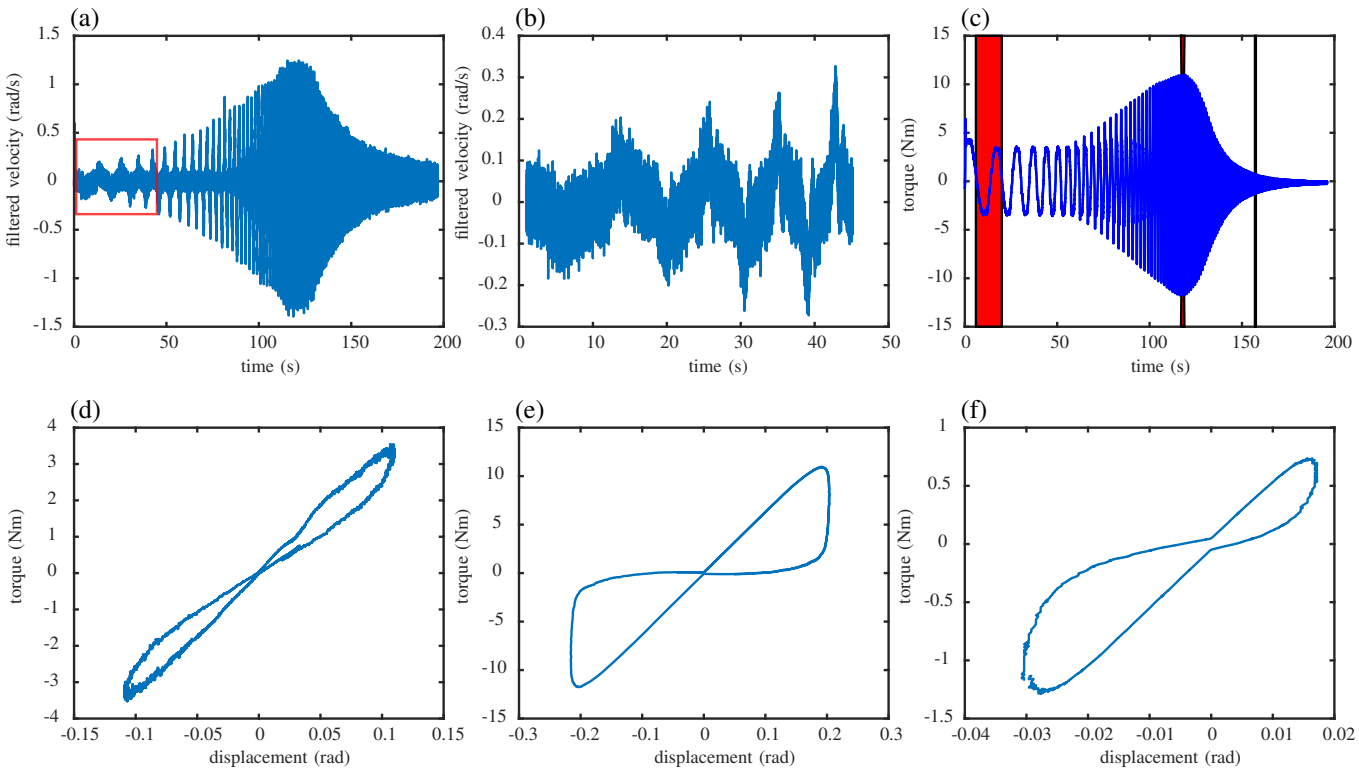

Fig. 6. Snapshot of a PHD impedance controller input-output profile

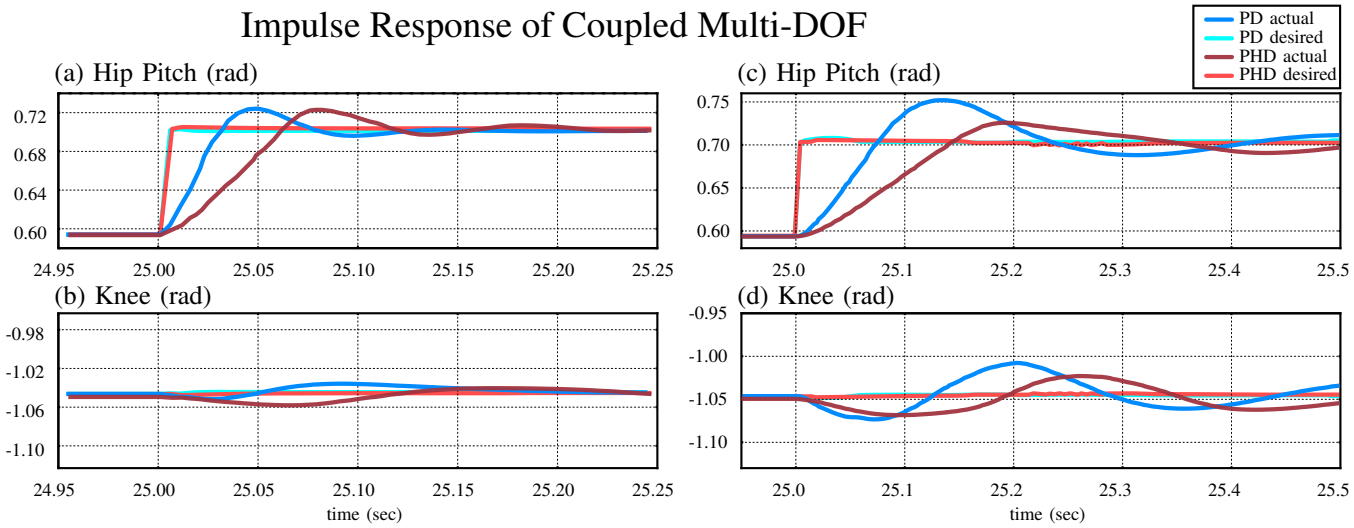

Fig. 7. Impulse Response

By using a PHD controller to compute the desired acceleration we are forcing the coupling of the robot's joints proportionally to the masses moved, additionally the hips orientation and center of mass task are set in Cartesian space which results in more coupled behaviors in joint space. Only the low-level torques τ_{PHD} originating from the PHD impedance controllers are truly decoupled. In order to test the robustness to external disturbances, we apply a sinusoidal force on the torso projected on the Z-axis of the robot's center of mass, visible as a blue ball in Fig. 9. Fig. 8 shows the reaction of the system to the aforementioned disturbance and we can retrieve the phenomena described in Fig. 8. Indeed, the torque profiles of the ankles look close to linear as (d), the hips pitch's profiles are hysteretic like (e), and the hip roll's compares well with (f). However, the knees do not compare well as they show an important bias torque even when crossing $\Delta q = 0$ and it is because of the coupling happening through the desired acceleration's PHD controller and the gravity compensation.

To demonstrate the conservation of the robustness to inertia

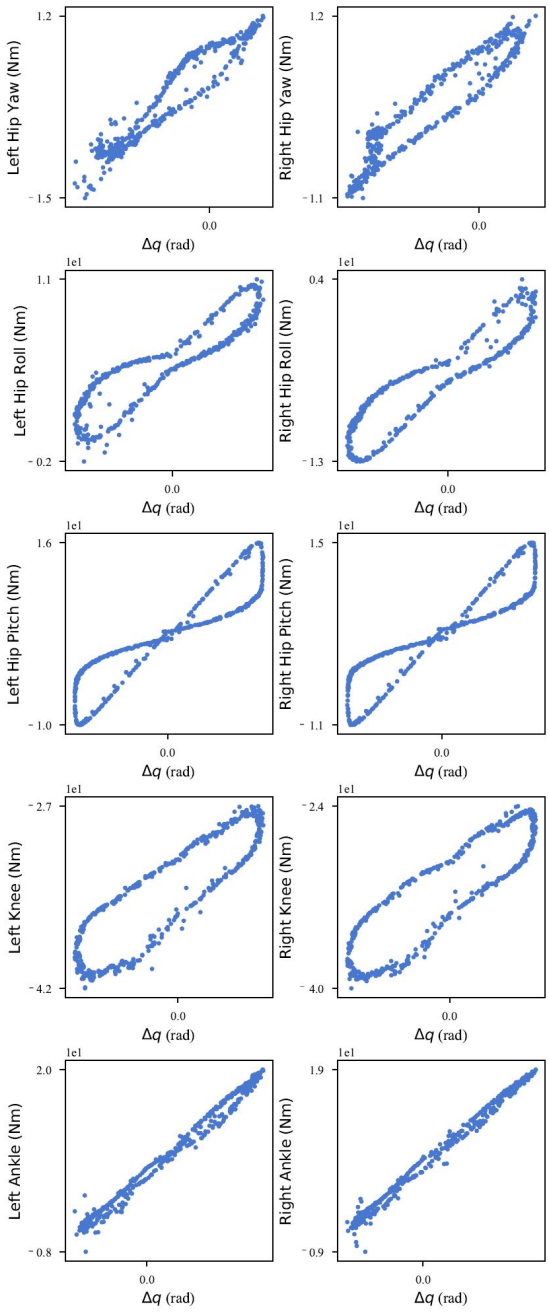

Fig. 8. Torque profiles in joint space

variations and to reduce the coupling effects in this multi-dof system, we give an impulse command to KinWBC to alter the pitch orientation of the hips while maintaining the roll, yaw, and center of mass positions. While it is challenging to decouple for our controller's study to resist external disturbances, we can still observe joint-level coupled frequency invariant damping in figure Fig. 7 as (a) and (b) show an equivalent overshoot, wherease (c) and (d) show the same impulse after increasing the hip's inertia and the PHD demonstrates a smaller overshoot than PD in both the hip pitch and the knee which is compensating for the COM variation.

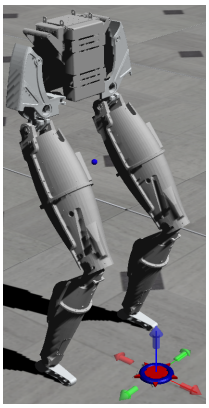

Fig. 9. DRACO

One can also notice that for a fixed stiffness and high d value, PHD had a slower step response than PD. This could be fixed by designing a separate variable k_{PHD}

$$k_{PHD} = \frac{k_{PD}}{1-\beta}, \quad \beta \neq 1, \tag{26}$$

such that the PHD controllers proactive stiffness matches that of the PD controller. While a bode plot will suggest the two systems should be matched in average stiffness, the proactive stiffness dominates for the step response.

V. Conclusion and Future Work

We have shown that a time-domain approximation of a complex stiffness is implementable and viable. Our PHD controller can be scaled and reliably used to achieve human-like mass-invariant damping ratios without estimating the mass. As a standalone controller, PHD proposes a different compromise than PD in the sense that its performance metrics is best defined in terms of resilience to inertia changes, a future implementations of PHD controllers for humanoid robots would benefit from a different WBC framework which more clearly allows analysis of the task-space stiffness, and which more reliably saturates the commanded task behavior to prevent foot-tilting, jumping, and slipping modes which made it difficult to measure the whole body damping ratio in our DRACO simulations. This implementation will notably allow for testing on the real robot and support future research in manipulation, haptics feedback and collision response in the context of human-robot interactions.

References

[1] M. Wang, T. Zan, Y. Yang, and R. Fei, "Design and implementation of nonlinear tmd for chatter suppression: An application in turning processes," *International Journal of Machine Tools and Manufacture*, vol. 50, no. 5, pp. 474–479, 2010.

[2] L. Tong, Y. Zhang, X. Zhou, A. Keivan, and R. Li, "Experimental and analytical investigation of d-type self-centering steel eccentrically braced frames with replaceable hysteretic damping devices," *Journal of Structural Engineering*, vol. 145, no. 1, p. 04018229, 2018.

[3] E. J. Perreault, R. F. Kirsch, and P. E. Crago, "Multijoint dynamics and postural stability of the human arm," *Experimental brain research*, vol. 157, no. 4, pp. 507–517, 2004.

[4] B. He, H. Huang, G. C. Thomas, and L. Sentis, "Complex stiffness model of physical human-robot interaction: Implications for control of performance augmentation exoskeletons," *arXiv preprint arXiv:1903.00704*, 2019.
[5] D. M. Dudek and R. J. Full, "Passive mechanical properties of legs from running insects," *Journal of Experimental Biology*, vol. 209, no. 8, pp. 1502–1515, 2006.
[6] J. A. Inaudi and J. M. Kelly, "Linear hysteretic damping and the hilbert transform," *Journal of Engineering Mechanics*, vol. 121, no. 5, pp. 626–632, 1995.
[7] J. A. INAUDI and N. MAKRIS, "Time-domain analysis of linear hysteretic damping," *Earthquake engineering & structural dynamics*, vol. 25, no. 6, pp. 529–545, 1996.
[8] N. Makris, "Causal hysteretic element," *Journal of engineering mechanics*, vol. 123, no. 11, pp. 1209–1214, 1997.
[9] A. Keivan, B. M. Phillips, M. Ikenaga, and K. Ikago, "Causal realization of rate-independent linear damping for the protection of low-frequency structures," *Journal of Engineering Mechanics*, vol. 143, no. 9, p. 04017058, 2017.
[10] T. J. Reid, "Free vibration and hysteretic damping," *The Journal of the Royal Aeronautical Society*, vol. 60, no. 544, p. 283283, 1956.
[11] Y. Karayiannidis, D. Papageorgiou, and Z. Doulgeri, "A model-free controller for guaranteed prescribed performance tracking of both robot joint positions and velocities," *IEEE Robotics and Automation Letters*, vol. 1, no. 1, pp. 267–273, 2016.
[12] M. Pi, Y. Kang, C. Xu, G. Li, and Z. Li, "Adaptive time-delay balance control of biped robots," *IEEE Transactions on Industrial Electronics*, 2019.
[13] Y. Zou and Z. Meng, "Immersion and invariance-based adaptive controller for quadrotor systems," *IEEE Transactions on Systems, Man, and Cybernetics: Systems*, 2018.
[14] J. Lee, M. X. Grey, S. Ha, T. Kunz, S. Jain, Y. Ye, S. S. Srinivasa, M. Stilman, and C. K. Liu, "Dart: Dynamic animation and robotics toolkit," *The Journal of Open Source Software*, vol. 3, no. 22, p. 500, 2018.
[15] J. Ahn, D. Kim, S. Bang, and L. Sentis, "Control of A High Performance Bipedal Robot using Liquid Cooled Viscoelastic Actuators," *arXiv preprint arXiv:1906.03811*, 2019.
[16] D. Kim, S. Jorgensen, J. Lee, J. Ahn, J. Luo, and L. Sentis, "Dynamic locomotion for passive-ankle biped robots and humanoids using whole-body locomotion control," *arXiv preprint arXiv:1901.08100*, 2019.